Hindawi Publishing Corporation
International Journal of Oceanography
Volume 2013, Article ID 403259, 11 pages
http://dx.doi.org/10.1155/2013/403259

Research Article

Internal Solitary Waves in the Brazilian SE Continental Shelf: Observations by Synthetic Aperture Radar

João A. Lorenzzetti and Fabian G. Dias

Divisão de Sensoriamento Remoto, Instituto Nacional de Pesquisas Espaciais (INPE), CP 515, 12227-010 São José dos Campos, SP, Brazil

Correspondence should be addressed to João A. Lorenzzetti; loren@dsr.inpe.br

Received 23 October 2012; Accepted 25 February 2013

Academic Editor: Robert Frouin

We present an analysis of internal solitary waves (ISWs) on the SE Brazilian continental shelf using a set of Envisat/ASAR satellite images. For the 17-month observation period, 467 ISW packets were detected. Most of observed solitons were associated to 4–6 ms^{-1} wind. The number of ISW packets shows a seasonal signal with a peak in summer, with higher concentration in the outer shelf in all seasons, followed by midshelf during the summer. Propagation direction of ISWs was predominantly onshore with packets separated by typical M_2 internal tide wavelengths (~10–40 km). The highest values of the barotropic tidal forcing F are concentrated at the shelf break between 200 and 500 m isobaths. These characteristics suggest that ISWs are formed from nonlinear disintegration of internal tides generated at the shelf break that propagate shoreward as interfacial internal waves. No significant change in the number of ISWs from spring to neap tides was observed in spite of significant tidal current variation (60%). Even not being a region of strong tides, this study shows that ISWs are a frequent and widespread feature, possibly playing a significant dynamic role, affecting biological production, sediment dispersion, and transport.

1. Introduction

Since the launch of SEASAT in 1978, numerous studies of oceanic internal solitary waves (ISWs) have been made using synthetic aperture radar (SAR) images. The availability of a great number of SAR satellite images has shown that ISWs are an ubiquitous oceanic phenomenon. They are frequently observed wherever tidal currents and stratification occur near significant seafloor topographic features, such as shelf break zones, plateaus, or sills [1]. Although a large number of remote sensing studies of ISWs have used SAR images, these features can also be observed in ocean color imagery [2] and in Sun glitter regions of visible images [3]. ISWs normally appear in SAR images as packets of 2–8 dark and bright stripes, with subsequent packets separated by distances corresponding to the wavelength of the internal tides (Figure 1) [1, 4].

At typical microwave frequencies used in SAR systems (1–10 GHz), the penetration depth of radar pulses in sea water, which is dependent on the complex permittivity, is restricted to less than about one centimeter [5]. Although practically a surface phenomenon, the backscattering of SAR electromagnetic pulses by wind-generated centimeter scale gravity-capillary surface waves (Bragg resonant waves) allows the visualization of ISWs, which are present tens of meters deep. Several physical mechanisms have been postulated as responsible for making ISWs visible in SAR images. In a pioneer work, [6] suggested as the main mechanism the hydrodynamic modulating effect of convergences/divergences of ISWs surface currents on the Bragg waves. Another mechanism was proposed by [7, 8], who showed that in low wind speed regions (less than 5 ms^{-1}), the ISW signatures in SAR images are strongly controlled by the effects of surface films or surfactants. More recently, [9] showed that wave breaking is also a major mechanism leading to the formation of surface signatures of ISWs in SAR images.

ISWs can play an important role in oceanic biological productivity. The passage of a train of ISWs can uplift the phytoplankton near the mixed-layer base, increasing light intensity and photosynthesis [10]. An enhancement in productivity can also occur by vertical mixing and upward flux of nutrients

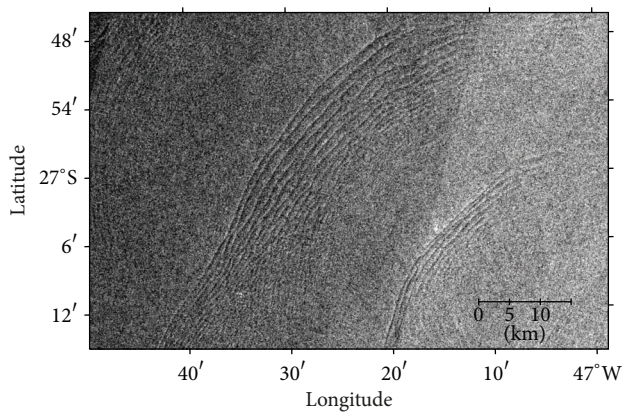

Figure 1: Example of two ISWs packets generated at consecutive tidal cycles observed on the Brazilian southeast coast. Image acquisition date: February 3, 2010; geographic position is indicated at insert box in Figure 2.

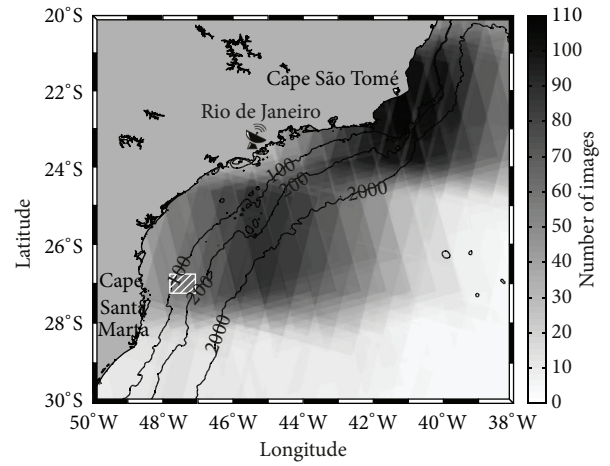

Figure 2: Study region with the number of ASAR scenes available in each area (see gray scale at right). Continuous black lines: isobaths in meters. White hatched rectangle represents geographic coverage of image in Figure 1. Small antenna indicates position of INPE's SAR data reception station.

during energy dissipation by internal wave breaking [11–14]. ISWs can as well affect sediment resuspension, producing turbidity signatures [15, 16] and inducing sediment transport [17]. Internal waves and solitons are reported affecting sound propagation. Anomalous sound propagation and acoustic transmission losses in the summer and in the coastal zone have been attributed to the resonance of the sound signal with ISWs [18].

ISWs have their origin in the baroclinic internal tides (ITs) which are forced by the deep ocean barotropic tide. The shelf break is the most important place for ITs generation. There, the flow of barotropic tidal currents interacts with steep bottom gradients producing large displacements of the isopycnals that start to propagate as ITs during tide reversals [19]. The most common form of ISWs generation is when IT energy, formed at the shelf break radiates horizontally as an interfacial internal wave in the thermocline/pycnocline. As the IT propagates onshore, it can disintegrate into ISWs in the form of solitons, which are able to maintain their shapes and velocities as the result of a balance between nonlinearity that tends to steepen their crests and dispersion that broaden them, much as an undular bore [20, 21]. The ISWs travel in the same direction as the generating ITs and are phase locked to their troughs [22]. In such cases, a remote generation region can normally be attributed to the observed ISWs.

Some ISW packets can appear locally, that is, well away from any specific topographic feature of origin as the shelf break. These are cases in which an IT energy ray reaches the thermocline after reflection in the bottom or at surface, producing large displacements in the thermocline. References [23, 24] reported such a case for the central Bay of Biscay, where the appearance of ISWs was associated to an IT energy beam generated at the shelf break that propagated downward, reflected at the bottom, and excited the thermocline near the location where the ISWs were found. Analyzing this local formation mechanism, [25] showed that a moderate developed thermocline is ideal for ISWs local generation. An IT energy beam propagates almost unimpeded through a too weak thermocline, or reflects back to deeper layers on a too strong one. In both cases, no significant perturbations are produced in the thermocline and no ISWs can be locally generated.

In situ observations of internal tide activity near the shelf break over the Brazilian southeast continental shelf were reported by [26]. Using the results of a three-dimensional tidal model implemented for the region, they showed that the baroclinic M_2 energy flux is, however, weak when compared to other regions known for strong internal tides and is predominantly offshore. In a following paper, [27] modeled the influence of Brazil Current (BC)—normally near the shelf break in this region—on the propagation characteristics of ITs. Results indicated that BC acts as a barrier to onshore propagation of internal tides generated over the upper slope, tending to reflect them back toward the open ocean.

Although these first studies of ITs on the SE Brazilian shelf did not indicate that ISWs could be significant over the shelf region, using satellite data [28] showed in a global atlas of ISWs the occurrence of these features in the region. The observed ISWs had characteristics similar to ISWs of other continental shelf regions around the world. More recently, with the availability of new SAR images for the region a much more significant presence of ISWs over the shelf than previous studies indicated became clear.

The purpose of the present work is, therefore, to clarify this issue and to contribute to a better picture of ISWs occurrence in this region. This is done by an analysis of a relatively large data set of SAR images for the region. Our goal is to extract from the data set, ISWs main space and time characteristics, such as speed, orientation, and wavelength and length along the crest, and to locate the likely generation sites of internal tide and subsequent solitons in the region. To the best of our knowledge, this is the first study of its kind for the SE Brazilian shelf.

2. Study Area

The study area is located between 20–30°S and 38–50°W in the subtropical western South Atlantic (Figure 2). Despite the availability of SAR scenes for the deep oceanic basin, our focus in this study is on the continental shelf and adjacent shelf break regions, where most of the ISWs were found. The continental shelf subregion is called the Southeast Continental Shelf (SECS). It presents smooth bottom topography with the shelf break depth between 120 and 180 m [29].

The SECS can be divided into three subregions with different physical characteristics: inner, mid, and outer shelf. The inner continental shelf (ICS) is totally mixed without any vertical stratification throughout the year. It extends from the coast to about the 30 m depth during the summer and to the 60 m during the winter. The mid continental shelf (MCS) is vertically stratified during the summer, with a strong seasonal thermocline, and extends from 30 m to 80 m depth in this season. During the winter, the MCS is narrow (confined between 60 and 80 m depth), or almost absent. The outer continental shelf (OCS) extends from the 80 m depth to the shelf break (~180 m); a permanent thermocline is present there all seasons. The Brazil Current (BC), a relatively weak western boundary current, is the main dynamic feature in the OCS. It flows southward along the slope from about 10°S until the subtropical convergence region (33–38°S) [30]. A strong mesoscale circulation, with BC meandering and eddies, is present in the OCS and slope [31, 32].

From mid to end autumn (April-May) and throughout the winter (June–August), all southern Brazilian coast and the south part of SECS are affected by a northward intrusion of low salinity waters from the La Plata river estuary, the so-called Plata Plume Water (PPW). The PPW extends more than 1000 km from the estuary and induces vertical stratification over the shelf in this region [33].

The semidiurnal lunar tidal constituent (M_2) is the main tidal component in the SECS [34]. Tidal amplitudes decrease southward from 0.35 m near Cape São Tomé to 0.1 m in Cape Santa Marta [30].

3. Data Set and Methods

The radar data set consisted of 264 C-band VV polarization images from the Advanced Synthetic Aperture Radar (ASAR) on board ENVISAT satellite of the European Space Agency (ESA). ENVISAT, a sun-synchronous polar orbit satellite, flying at an orbit altitude of about 800 km with a repeat cycle of 35 days, was launched on March 1, 2002 and operated until April 2012. Images used in this investigation were acquired in January 2009 and from September 2009 to December 2010 by the National Institute for Space Research—INPE's receiving station in Brazil (22°40′58″S; 45°00′07″W; see position indicated by a small antenna in Figure 2). SAR raw data was processed at station site to Level 1b format using the ACS (Advanced Computer Systems) SAR processor. The data gap between January and September of 2009 was caused by initial technical difficulties found during implementation of station. Data analysis was limited to the end of 2010 by technical problems encountered subsequently which could not be resolved in time for the present investigation. The product used for analysis was of medium resolution (pixel size of 75 m) and wide swath of 400 km. Data set contained almost the same number of ascending (129) and descending (135) orbit images.

The data set covered predominantly the SE Brazilian continental shelf and adjacent offshore waters between 20° and 28°S (Figure 2). Between 28° and 30°S the number of images was considerably lower (about 7 times less) than on the remaining region; so the results for this area are statistically less robust. A seasonal analysis of the data set shows that winter time (JAS) images prevailed in the northern portion of the region, while images in other seasons prevail toward the south.

For each SAR image, detection of ISWs was done by visual analysis of subregions which had been digitally processed, registered to a latitude/longitude projection, and enhanced. Each detected ISW packet had its average center coordinates recorded and all main characteristics annotated. The wind speed over each observed internal wave packet was estimated using ASCAT scatterometer data at 12.5 and 25 km resolution cells obtained from [35]. A maximum acquisition time difference of 5 hours between scatterometer winds and ASAR images was guaranteed. The "climatologic" monthly mean wind speed was downloaded from [36], which is based on 10 years of QuickScat data. Bathymetry for the study region was the ETOPO 2, at a spatial resolution of 2′, which was obtained from [37].

The components of the maximum barotropic tidal velocity for M_2 constituent were obtained from the 1/4° resolution model OTIS—Oregon State University Tidal Inversion Software [38]. The velocity components were linearly interpolated onto the finer grid of ETOPO2 with resolution of 2′. The Brunt-Väisälä frequency (N) was calculated from objectively analyzed monthly temperature and salinity vertical profiles obtained from World Ocean Atlas 2009 (WOA09) [39], at a resolution of 1°.

Using the described data, the barotropic body force F [40] was calculated for the summer period (JFM). F is the forcing term of the baroclinic internal tide and is associated with the vertical motions produced by the horizontal barotropic tidal flow interacting with bottom topography in the presence of vertical stratification. The amplitude of depth-integrated body force is given by

$$F = \frac{1}{\omega} Q \cdot \nabla \left(\frac{1}{h} \right) \int_H^0 z N^2 (z)\, dz, \tag{1}$$

where ω is the tidal angular frequency (rad s^{-1}), z is the upward vertical coordinate ($z = 0$ at sea surface), $N(z)$ is the local Brunt-Väisälä frequency, Q is the barotropic flux vector $Q = (Q_x, Q_y) = (u_1 H, v_1 H)$, u_1 and v_1 are the zonal and meridional components of the barotropic tidal velocity, H is local depth, and $h(x, y)$ is the ocean bathymetry.

4. Results and Discussion

From the set of 264 SAR images, about 34% (89 images) contained some ISW signature. As a measure of comparison,

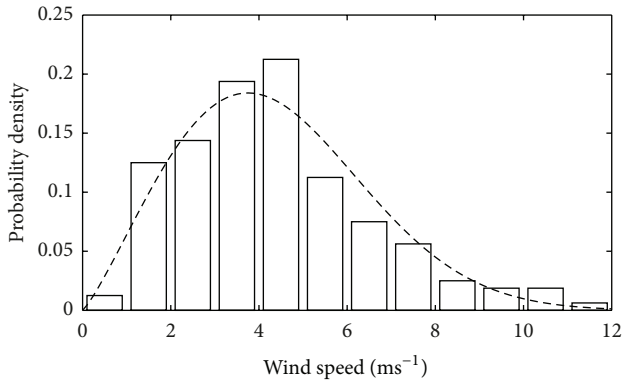

Figure 3: Histogram of wind speed observed over 160 ISW packets for the period 2009-2010. Dashed line: a best fit of a Weibull pdf distribution.

[41] found 5% out of 2600 images with some ISWs for the Norwegian shelf utilizing ERS1-2 and Radarsat-1 images with different swaths. In our study region, a total of 467 ISWs packets were detected for the analyzed period. The number of ISW packets was almost equally distributed among ascending (232 packets) and descending (235 packets) orbit images. Corresponding sea surface wind speed was recovered for 160 of them.

4.1. Wind Effect on ISW Detection and Seasonal Variability. Sea surface wind is an important factor for internal wave imaging according to SAR image theories. According to [42], ~3 ms^{-1} would be the weakest wind required for SAR imaging of ISWs. This low wind limit is, however, not so clearly defined. According to [7], for *C* band radar images, internal waves can still be seen as bright bands in a dark background in winds under 2 ms^{-1} due to a resonance mechanism of dm-waves with the ISW. As the wind becomes strong, the ISW modulation depth (the anomaly of backscatter from its mean value) is significantly reduced, making it harder to observe the ISWs in SAR images. Simulations done by [43, 44] indicate that for winds higher than about 7-8 ms^{-1} the ISW contrast between maximum and minimum signals relative to the normal sea clutter becomes very weak, making the detection difficult.

Figure 3 shows the histogram of wind intensity over 160 observed ISW packets for the study period and the Weibull probability density function (pdf) fit (shape factor $k = 2.19$ and scale factor $c = 4.96$), leading to mean and standard deviation wind values of 4.4 ms^{-1} and 2.1 ms^{-1}, respectively [45].

Approximately 97% of the observed ISW packets were associated with winds below 10 ms^{-1} although a few were detected at wind speeds of about 11-12 ms^{-1}. Similar result is reported by [46] for the northern South China Sea. Most of ISWs were observed at winds between 2.3 and 6.5 ms^{-1} (mean ± 1 sd), which according to the pdf correspond to a probability of 67% of the data set. This result is similar to the theoretical limits put by [42–44].

Summer and winter spatial distributions of wind speed for the study region based on 10 years of QuickScat data are depicted in Figure 4. As expected, wind speed decreases toward the coast and is weaker during the summer. For summer and winter, winds below 7 ms^{-1} are generally observed over the continental shelf. The seasonal average minimum winds are present during the summer (January) between Rio de Janeiro (22.9°S) and São Sebastião (23.75°S) with values close to 4 ms^{-1}; during the winter this minimum regional cell is displaced to southwest with minimum winds of 4.5 ms^{-1}. It is well known that the presence of surface films can reduce short-scale roughness and radar backscatter, inducing a negative bias in the retrieved surface wind via Geophysical Model Function used. However, by our experience in analyzing SAR images for this region, we consider that the minimum wind regions referred to above are not the result of this effect. These regional minimum wind centers are more likely the combined result of the presence of a high mountain range very close to shoreline, the orientation of coastline and the NE and E wind directions prevailing in the summer and E and SW during the winter. In the wintertime, average wind speeds above 8 ms^{-1} are observed south of 28°S. These wintertime higher winds are normally associated with the passage of cold fronts which brings S/SE average winds of 8 ms^{-1} [47]. These results indicate that typical wind speeds observed over the continental shelf at SECS are adequate for SAR observations of ISWs, and except for extreme meteorological events or after the passage of strong cold fronts, wind should not be a limiting factor.

To get a sense of the seasonal variability, we present in Figure 5 the mean number of ISWs packets observed per image and for different seasons. A clear seasonal cycle of ISWs observed in the region is present, with a dominance of wave packets during the summer as compared to winter and autumn; a small but visible increase is seen for the spring season. The high standard deviations are probably associated to the variability of conditions necessary for the generation and observation by SAR of ISWs. A fair number of images showed no ISWs whilst some had 18 ISWs packets.

4.2. Tidal Variability and ISW Generation. According to results of the OTIS tidal model, barotropic tidal currents over the shelf break in the region are about 60% stronger during spring tides. Since ISWs are generated by ITs, which are formed by the barotropic tide, it should be expected a positive correlation between observed ISWs and the fortnight tidal cycle. Surprisingly, separating the ISWs according to the phase of tidal cycle at time of image acquisition, it was verified that a few more ISWs packets were observed during neap tides than during spring tides. Considering that similar number of images was available for both tidal periods, we can conclude that no correlation exists in the region between the number of ISWs packets and the strength of tidal currents. A similar behavior is reported by [48] for the New Jersey North America east coast. The suggested explanation for this behavior was the presence of remotely generated shoaling internal tides which could induce significant changes in local internal tide generation. If the phase of shoaling IT is randomly

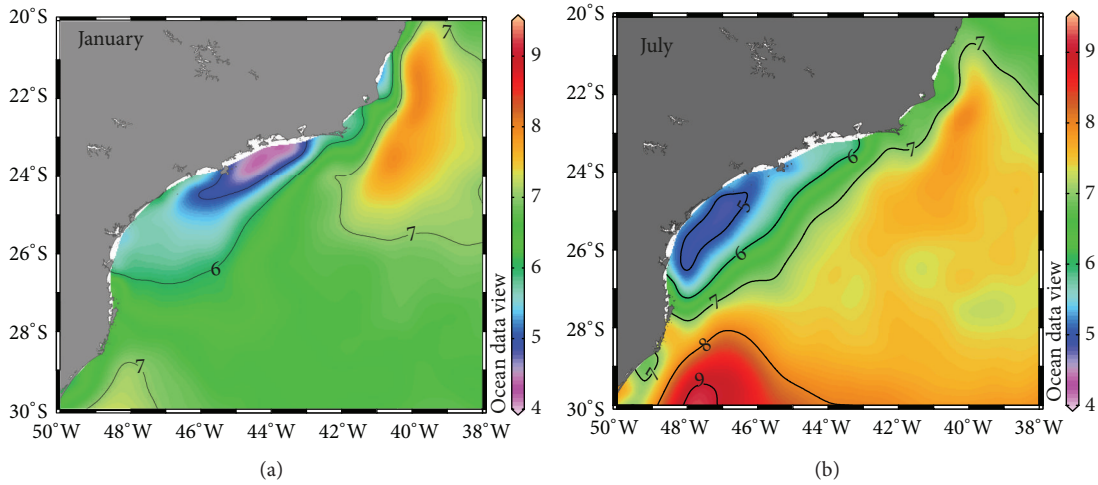

Figure 4: Spatial distribution of mean summer (January) and winter (July) wind intensity for the study region based on 10 years of QuickScat data.

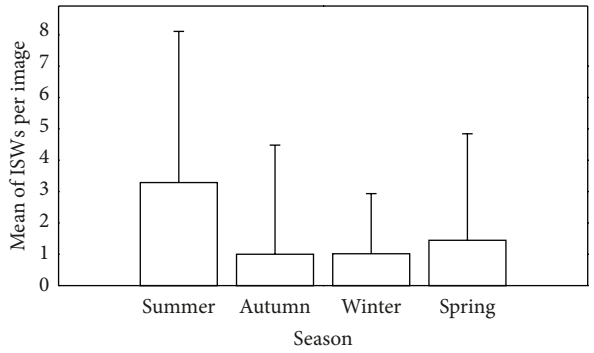

Figure 5: Average number of ISWs packets per scene and one standard deviation (vertical bars).

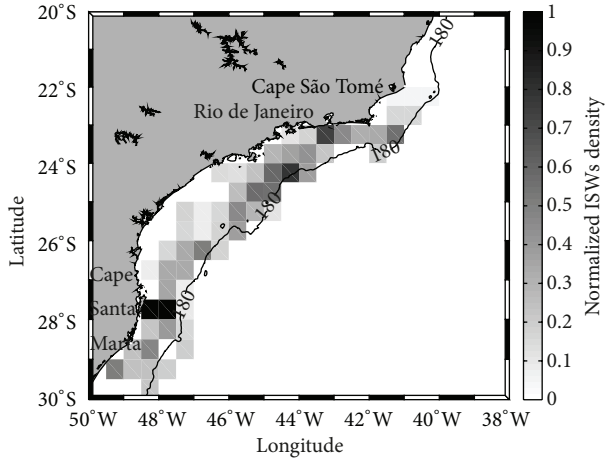

Figure 6: Summertime spatial distribution of ISWs. Values are normalized (see text) number of ISWs per number of scenes for the period.

changed by interaction with currents and mesoscale features, its pressure perturbations can interact constructively or destructively with barotropic tidal velocities, reinforcing or inhibiting internal tides generation. Lack of correlation of ISWs to tidal phase is also reported by [49, 50] on the Portuguese shelf. In this region, large amplitude ISWs with similar amplitudes were observed during neap and spring tides even though the barotropic tide changed by a factor of 2. Their explanation for this behavior was that the ISWs theoretical limiting amplitudes had already been achieved during the neap tides. In our case, it is difficult to say which of these theoretical explanations would be more suitable considering the limitations of the available data set.

4.3. Spatial Distribution and Direction of Propagation. The spatial distribution of observed ISWs is presented in Figures 6 and 7. The results were calculated in cells of $0.5^\circ \times 0.5^\circ$ lat/long, corresponding to a typical length of ISWs crests. At each cell, the total number of ISWs packets was divided by the total number of satellite images covering the same area and period. The maximum number found for the region was set to one and used for normalization so that scales vary from 0 to 1 for both figures. Although a fair number of satellite scenes covered the deep ocean (see Figure 2), almost all of the ISWs packets were observed in the continental shelf at depths lower than 200 m. For the summer period (Figure 6), except at the northernmost portion of the region, north of 22°S where no ISWs were detected, solitons were seen throughout the region. Regional maximum concentrations of ISWs were near the islands of Florianópolis (27.8°S) and São Sebastião (23.75°S) as well as near Rio de Janeiro (22.9°S). Spring season ISWs spatial distribution (not shown) has a very similar pattern.

The spatial distribution of ISWs for the grouped autumn and winter seasons is shown in Figure 7. The reason for joining these two seasons was first that they seem to have similar environmental conditions for ISWs generation and SAR observation (Figure 4) and second that the number of

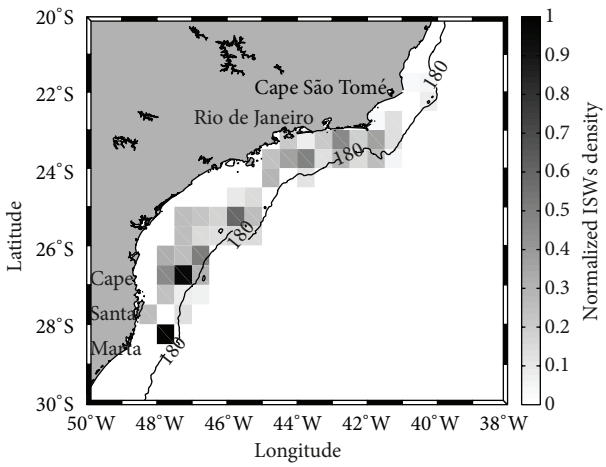

Figure 7: Same as Figure 6 but for grouped autumn and winter images.

ISW packets observed in winter was too low to produce a significant separate analysis.

Similar to the summer period, during autumn and winter ISW packets were observed all over the study area, but with a lower number of ISWs per scene. The seasonal decrease of observed ISW packets in the winter seems to be related to the seasonal decrease in the vertical stratification in the period (Figure 8).

The very low number of ISW packets south of 28°S can be, however, somewhat negatively biased; no winter images were available in this area and only a low coverage was obtained during autumn. Additionally, during autumn and winter the average wind speed increases, staying over 7 ms^{-1} south of 28°S (see Figure 4), and as discussed before, decreasing the visibility of ISWs in SAR images. Stratification in the southern sector of this region is also singular. The PPW northward intrusion in this period causes a salinity-induced stratification and an inverted thermocline [33, 51]. Numerical experiments done by [52] indicate that vertical stability solely caused by salinity cannot produce, support, or augment the internal wave oscillations. Their results also indicate that horizontal convergence/divergence of surface currents—required for the manifestation of internal waves at the surface—are inhibited in the presence of temperature inversion. Therefore, we suppose that the PPW intrusions might also contribute to the low number of ISWs south of 28°S.

The frequency of ISW observations as a function of local depth is presented in Figure 9 for two periods: spring/summer (son/djf) and autumn/winter (mam/jja). For both periods, most of the ISW packets were observed between the 80 and 160 m isobaths at the outer shelf and shelf break regions, followed by midshelf occurrences. Inshore, the 40 m depth—at the inner shelf—the percentage of observed ISWs was very low. Toward the deep ocean, no ISWs were observed beyond the 500 m isobath.

The prevailing propagation direction of ISWs (Figure 10) was onshore at 319° (measured clockwise from north). Most of the ISWs were observed propagating normal to the local bathymetry toward the coast as a result of wave refraction and tidal advection. Near 26°S and 23.5°S, where the 180 m isobath is oriented almost in an eastwest direction, it is possible to observe ISWs propagating northward. A very few anomalous cases of ISWs propagating offshore were observed. These cases were concentrated especially near 23.5°S and 41.5°W. A few cases of ISWs propagating southward were observed in the northern part of the domain following the topography.

4.4. Formation Region and Likely Generation Mechanism. Considering the spatial distribution and the prevailing onshore direction of propagation of ISWs, it is likely that they are being formed at the shelf break. However, the combination of local depth gradients, with dominant direction and strength of tidal currents and stratification can favor specific places as main generation sites of ITs. To estimate these probable generation sites, we calculated the depth-integrated-amplitude of the barotropic body force (F) using ETOPO2 bathymetry, the summer mean stratification, and maximum value of M_2 tidal current component (1). This variable has been extensively used as a good indicator of the source regions of internal tides [53–56]. The spatial distribution of the depth-integrated amplitude of F is shown in Figure 11.

As anticipated, the highest values of F are concentrated between the 200 and 500 m isobaths at the slope, mostly in response to the steep topography gradients of this region. This strongly indicates the shelf break as the main region for IT generation in SECS. Three areas concentrate the highest F values: one between 25 and 26°S, one between 23 and 24°S, SE of Cabo Frio, and a more extensive one between 20 and 22.5°S. Although Figure 11 suggests north of 24°S as being a favorable region for IT generation, one or more mechanisms could be acting to prevent the generation (or observation) of ISWs north of 22°S, since very few ISW packets were observed in this northern sector throughout the year (Figures 6 and 7). For the region between 20°S and 23°S, [57] show that the Brazil Current inshore thermal front is positioned in the outer shelf region, inshore the 200 m isobath. As discussed by [27], it is possible that ITs generated at the shelf break in this region are being reflected back to deep ocean by the BC before disintegrating into ISWs. Other specific characteristics of this region, such as a narrow continental shelf, a weaker stratification (Figure 8), and stronger winds (Figure 4) may be contributing to hinder ISWs generation/observation.

Considering the results presented above, it is reasonable to assume that the ITs in the SECS are being generated at the shelf break and show a clear onshore propagation. We are not excluding here offshore propagation of ITs as indicated by [27]; the point is that we only observed a very small number of solitons with offshore propagation in the region. Thus, it is very probable that the ISWs observed in the continental shelf are caused by a nonlinear disintegration of interfacial internal tides propagating shoreward.

4.5. Some ISW Characteristics. The observed solitons are phase locked to the troughs of the ITs so that sequential ISW packets must be separated by the ITs wavelength [58].

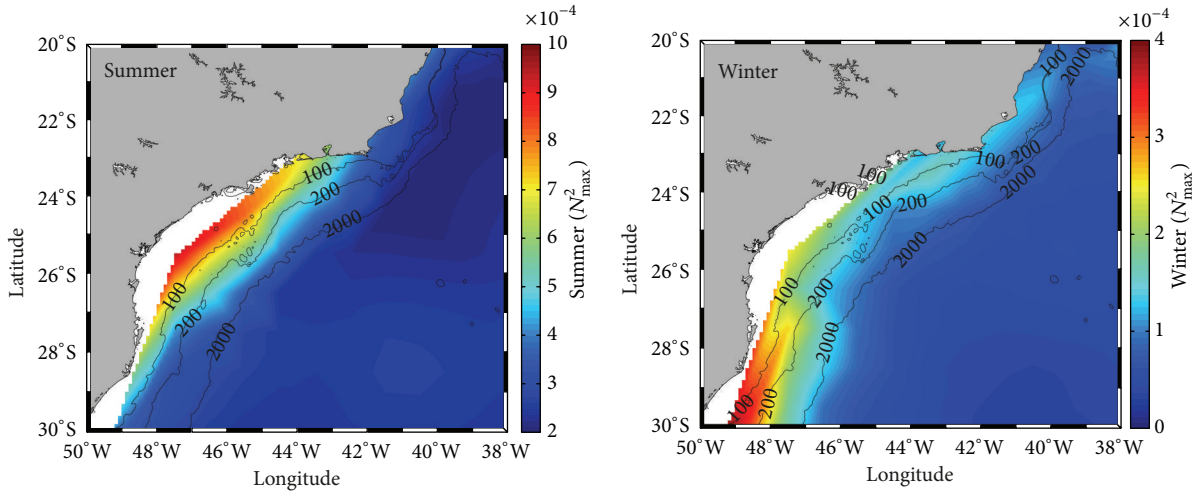

Figure 8: Climatological seasonal fields of maximum Brunt-Väisälä square frequency (N^2) for the study region. Data source: World Ocean Atlas 2009.

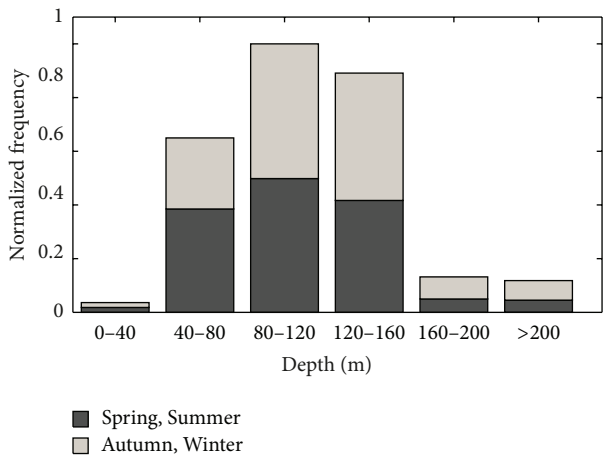

Figure 9: Observed seasonal occurrence of ISW packets as a function of local depth.

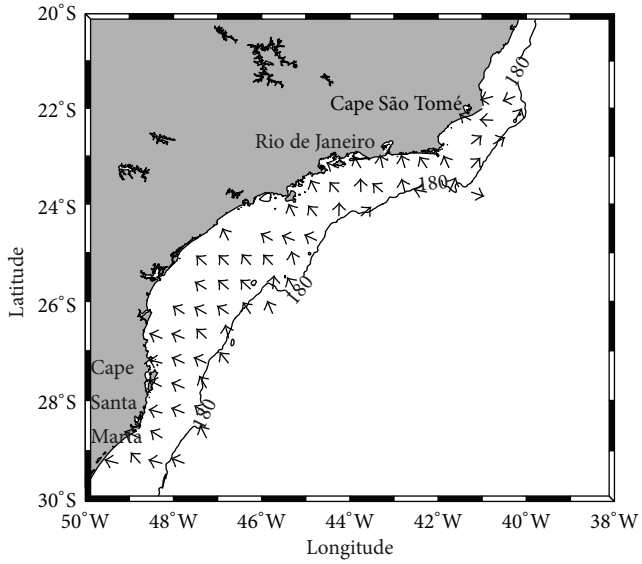

Figure 10: Average propagation direction (vectors) of ISWs observed in the SECS.

Sequential packets of ISWs are very similar in shape and direction of propagation and their separation can be easily measured in SAR images from the center of the first soliton of each packet. A typical IT wavelength scale can also be estimated as NHT/π, where N is the typical buoyancy frequency, H is the water depth, and T the tidal period [27, 59]. A comparison of these typical IT wavelengths, calculated using $T = 12.42$ h (M_2 tidal period), the climatological values of N, and local depth of observed solitons, against measurements of distance of sequential packets of ISWs is depicted in Figure 12. Albeit an anticipated scatter due to the simplifications assumed, a positive correlation between estimated and observed wavelengths is verified. We consider that this result goes in favor of the hypothesis that first, the ISWs observed in the region by SAR are strongly forced by the semidiurnal lunar tidal component, and second that the N values, as given by the WOA09 data set, are a reasonable approximation of the vertical stratification for the region.

Assuming that sequential ISW packets are generated at each M_2 tidal cycle, the mean phase speed of ISWs can be estimated dividing the measured distances of sequential solitons by the M_2 tidal period [60]. The result of this simple method is presented in Figure 13. The overall mean speed was 0.64 ms^{-1} with standard deviation (std) of 0.16 ms^{-1}. The maximum phase speed did not exceed 1.04 ms^{-1}. For spring and summer, the propagation speed was about 0.66 ms^{-1} with std. of 0.16 ms^{-1}, and for autumn and winter was slightly lower, 0.57 ms^{-1} with std. of 0.08 ms^{-1}, due to the weaker stratification. Similar values of phase speed have been

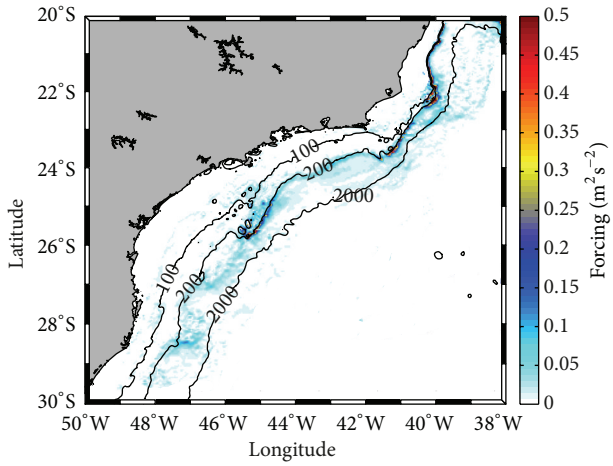

Figure 11: Depth integrated amplitude of M_2 barotropic tidal force field F.

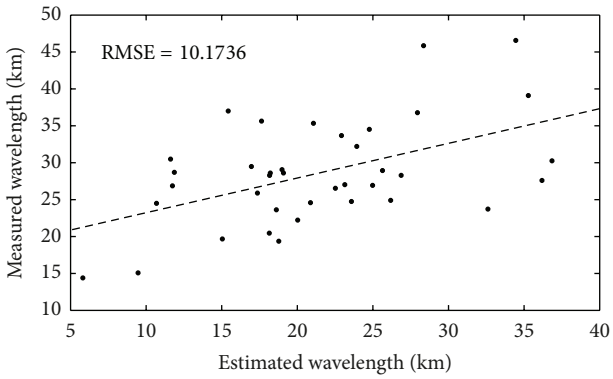

Figure 12: Theoretically estimated M_2 ITs wavelengths as NHT/π (horizontal axis) versus wavelength obtained from sequential ISWs packets (vertical axis).

observed in other continental shelves [1, 41, 61, 62] although much greater values, on the order of 2.5 ms^{-1}, have been reported in deeper areas [19].

The wavelength of the ISWs (i.e., the intersoliton separation) was measured for the first three solitons of the packets. A larger number of measurements for the first soliton was done since generally for the rear of the packets the signatures were normally weaker or very noisy. The first soliton average wavelength was 1.04 km with a maximum value of 2.36 km and a std. of 0.44 km. To the rear of the packets, the wavelengths decreased. The second and third solitons showed average wavelengths of 0.9 and 0.85 km, with std. of 0.42 and 0.37 km, respectively. The amplitudes of the solitons in the ISWs packets decrease from the front to the back of the packets. Since the velocity of a soliton is directly proportional to its amplitude, distances between one wave crest and the next decreases toward the back of the packet [1]. The higher wavelength standard deviation for the first solitons is also a result of their higher degree of nonlinearity and sensibility to slight variations in the stratification [43]. The values of wavelength did not change significantly between seasons.

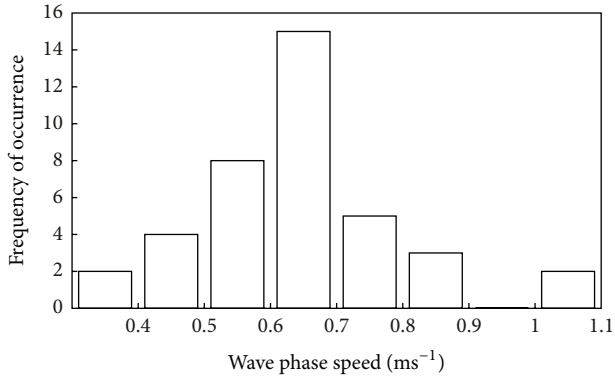

Figure 13: Histogram of phase speeds of ISWs estimated from the separation of sequential ISW packets.

The along-crest lengths were measured for the first soliton of the packets as this tends to be longest one. The mean observed length was 43.5 km with a standard deviation of 28 km. The maximum length was 152.5 km, but about 90% of the ISWs had along-crest lengths under 80 km. These lengths are typical of continental shelf ISWs [63]. However, much larger values have been reported in some places as in South China Sea [46, 64] and in the Mascarene ridge in the Indian Ocean [65] with along-crest lengths in excess of 200 km and 350 km, respectively.

5. Summary and Conclusions

A study of the space/time variability and main characteristics of oceanic ISWs off the Brazilian Southeast coast was carried out using a set of Envisat ASAR images. A summary of main results obtained is presented in Table 1.

Analysis of concomitant scatterometer wind data (max 5 h apart) showed that most of observed ISWs packets were associated with winds between 3 and 6 ms^{-1}; very few solitons were detected for wind speeds above 10 ms^{-1} (Figure 2). Contrary to a generally assumed 3 ms^{-1} weakest wind threshold for SAR observations, a few solitons were still visible at winds near 1 ms^{-1}, a fact also observed by [7]. Considering the wind speed climatology for the region (Figure 3), we can say that this variable should not be a complicating factor for ISW observation by SAR.

Summer was the season with the highest number of ISWs, more than three times the frequency of ISWs occurrence for autumn and winter. Summer stratification seems to be the main factor for such high concentration of ISWs in this season. Previous studies show that vertical stratification is present in the region from the outer shelf up to the inshore limit of the midshelf during the summer season; during the winter the midshelf practically disappears and stratification is concentrated in the outer shelf [30]. The high standard deviations (Figure 5) indicate that these waves depend on specific and changing environmental conditions for their generation as well as for observation by SAR. The presence of ISWs in all seasons confirms that vertical stratification is present even in winter, at least in the outer shelf and slope

Table 1: ISWs main characteristics in the SECS obtained from SAR imagery.

	Mean	Std. Deviation	Maximum	Minimun
Wind speed over ISWs (ms^{-1})	4.4	2.1	11.43	0.66
Local depth of occurrence (m)	111	51	509	14
Direction of propagation (degrees)	319	—	—	—
ISW propagation speed (ms^{-1})	0.64	0.16	1.04	0.32
Wave crest length (km)	43.5	28	152.5	10.5
Wavelength 1st soliton (km)	1.04	0.44	2.36	0.3
Wavelength 2nd soliton (km)	0.9	0.42	2.11	0.22
Wavelength 3rd soliton (km)	0.85	0.37	1.7	0.32
Wavelength of Internal Tide (km)	28.6	6.94	46.57	14.4

regions, a fact confirmed by N^2 climatology (Figure 8). The very small number of ISW packets observed in the inner shelf was expected considering that this is a well-mixed region all year round (Figure 8) and therefore not supporting the presence of internal waves.

The high number of observed ISW packets in the SECS indicates that they are generated every tidal cycle all year round. After formation, they propagate toward the coast and eventually dissipate by breaking, inducing turbulence and mixing. We raise here a hypothesis—yet to be tested—that a continuous ISWs breaking in the region could be acting together with wind mixing to maintain the inner shelf well mixed throughout the year.

The ISWs were well distributed in the north/south direction along the SECS all year round, except north of 22°S where the observation of ISWs was always low (Figures 6 and 7). We conjecture that this is probably a combined result of weak stratification, narrow continental shelf, stronger winds, and the Brazil Current intrusion over the outer shelf, reflecting ITs back to deep ocean. The outer continental shelf is where most of the ISW packets were observed (Figure 9); 74% of the summer and 84% of the winter ISWs were observed in this region. This seems to be linked to the presence of a permanent thermocline there. The mid continental shelf supports ISWs during the summer and spring; during the winter it is very narrow or almost absent. Shoaling is also a major mechanism contributing to the decrease of ISWs shoreward or their absence in the inner shelf.

The number of observed ISW packets did not change significantly between spring and neap tides despite a 60% variation of tidal currents. Similar cases have been reported elsewhere. This behavior has been explained by either an interaction of remotely generated shoaling baroclinic tides with local barotropic tides or by the fact that the limiting magnitude of the IT has already been reached during neap tides. Our data set is insufficient to make any statement in this regard for the region; numerical modeling and *in situ* data acquisition are needed before any conclusion can be drawn.

The highest values of the M_2 barotropic tidal forcing F are concentrated at the shelf break between 200 and 500 m isobaths (Figure 11). Almost all of the ISW packets showed onshore propagation (Figure 10), with sequential packets typically separated by distances on the order of the M_2 IT wavelengths (~10–40 km). These characteristics strongly indicate that the observed solitons are formed by nonlinear disintegration of shoreward propagating interfacial ITs formed at shelf break. Analyzing the slopes of M_2 IT ray characteristics for the region ($\alpha = (\omega^2 - f^2)/(N^2(z) - \omega^2)$) against topography gradient (γ), [27] show that slope is near to the critical condition for IT generation ($\alpha \sim \gamma$) at approximately 800 m depth. IT energy ray characteristics were modeled propagating both seaward and shoreward (Figure 12 of [27]). Therefore, sporadic "local" ISW generation at the shelf by IT energy rays exciting oscillations in the thermocline after reflection at bottom or surface should not be excluded if stratification conditions are adequate [25].

The mean phase speed of ISWs calculated from sequential packets was 0.64 ms^{-1} (Figure 13), being just slightly higher during summer and spring as compared to autumn and winter. Theoretical solutions show that higher speeds should be associated with stronger vertical stratification [66]. Average wavelength was about 1.04 km for the first soliton, decreasing to 0.85 km on the third as a result of nonlinearity. The average along-crest length was 43.5 km, with a maximum of 152.5 km.

Finally, we may say that despite not being a region of strong internal tides and having the presence of a western boundary current—Brazil Current is a permanent feature at the outer shelf—the analysis of ASAR data set revelead that ISWs are a ubiquitous feature in this region and, therefore, may play a relevant dynamic role in the SECS and possibly affecting biological production, sediment dispersion, and transport.

Acknowledgments

The authors would like to thank Petrobrás/Cenpes in the name of Dr. Cristina Bentz and ANP (National Brazilian Petroleum Agency) for supporting the installation and maintenance of the satellite reception station used for the acquisition and processing of the SAR images used in this paper. The second author thanks INPE for providing its facilities and CNPq (Process no. 130517/2010-0) for his financial support during his graduate program activities. The authors appreciate the helpful comments of two anonymous reviewers which contributed to improve this paper.

References

[1] J. R. Apel and F. I. Gonzalez, "Nonlinear features of internal waves off Baja California as observed from the Seasat imaging radar," *Journal of Geophysical Research*, vol. 88, no. 7, pp. 4459–4466, 1983.

[2] J. C. B. da Silva, A. L. New, M. A. Srokosz, and T. J. Smyth, "On the observability of internal tidal waves in remotely-sensed ocean colour data," *Geophysical Research Letters*, vol. 29, no. 12, pp. 1–10, 2002.

[3] C. R. Jackson, "Internal wave detection using Moderate Resolution Imaging Spectroradiometer (MODIS)," *Journal of Geophysical Research*, vol. 112, no. C11012, 2007.

[4] J. C. B. da Silva, A. L. New, and A. Azevedo, "On the role of SAR for observing "local generation" of internal solitary waves off the Iberian Peninsula," *Canadian Journal of Remote Sensing*, vol. 33, no. 5, pp. 388–403, 2007.

[5] F. T. Ulaby, R. K. Moore, and A. K. Fung, *Microwave Remote Sensing: Active and Passive*, vol. 3, Artech House, Norwood, Mass, USA, 1986.

[6] W. Alpers, "Theory of radar imaging of internal waves," *Nature*, vol. 314, no. 6008, pp. 245–247, 1985.

[7] J. C. B. da Silva, S. A. Ermakov, I. S. Robinson, D. R. G. Jeans, and S. V. Kijashko, "Role of surface films in ERS SAR signatures of internal waves on the shelf 1. Short-period internal waves," *Journal of Geophysical Research C*, vol. 103, no. 4, pp. 8009–8031, 1998.

[8] J. C. B. da Silva, S. A. Ermakov, and I. S. Robinson, "Role of surface films in ERS SAR signatures of internal waves on the shelf 3. Mode transitions," *Journal of Geophysical Research C*, vol. 105, no. 10, pp. 24089–24104, 2000.

[9] V. Kudryavtsev, D. Akimov, J. Johannessen, and B. Chapron, "On radar imaging of current features: 1. Model and comparison with observations," *Journal of Geophysical Research C*, vol. 110, no. 7, pp. 1–27, 2005.

[10] M. A. Evans, S. MacIntyre, and G. W. Kling, "Internal wave effects on photosynthesis: experiments, theory, and modeling," *Limnology and Oceanography*, vol. 53, no. 1, pp. 339–353, 2008.

[11] R. D. Pingree and G. T. Mardell, "Slope turbulence, internal waves and phytoplankton growth at the Celtic Sea shelf-break," *Philosophical Transactions of the Royal Society of London A*, vol. 302, pp. 663–682, 1981.

[12] H. Sandstrom and J. A. Elliott, "Internal tide and solitons on the Scotian Shelf: a nutrient pump at work," *Journal of Geophysical Research*, vol. 89, no. 4, pp. 6415–6426, 1984.

[13] P. M. Holligan, R. D. Pingree, and G. T. Mardell, "Oceanic solitons, nutrient pulses and phytoplankton growth," *Nature*, vol. 314, no. 6009, pp. 348–350, 1985.

[14] J. N. Moum, D. M. Farmer, W. D. Smyth, L. Armi, and S. Vagle, "Structure and generation of turbulence at interfaces strained by internal solitary waves propagating shoreward over the continental shelf," *Journal of Physical Oceanography*, vol. 33, no. 10, pp. 2093–2112, 2003.

[15] D. Bogucki, T. Dickey, and L. G. Redekopp, "Sediment resuspension and mixing by resonantly generated internal solitary waves," *Journal of Physical Oceanography*, vol. 27, no. 7, pp. 1181–1196, 1997.

[16] L. S. Quaresma, J. Vitorino, A. Oliveira, and J. da Silva, "Evidence of sediment resuspension by nonlinear internal waves on the western Portuguese mid-shelf," *Marine Geology*, vol. 246, no. 2-4, pp. 123–143, 2007.

[17] A. D. Heathershaw, "Some observations of internal wave current fluctuations at the shelf-edge and their implications for sediment transport," *Continental Shelf Research*, vol. 4, no. 4, pp. 485–493, 1985.

[18] J. Zhou and X. Zhang, "Resonant interaction of sound wave with internal solitons in the coastal zone," *Journal of the Acoustical Society of America*, vol. 90, no. 4 I, pp. 2042–2054, 1991.

[19] J. R. Apel, J. R. Holbrook, A. K. Liu, and J. J. Tsai, "The Sulu sea internal soliton experiment," *Journal of Physical Oceanography*, vol. 15, no. 12, pp. 1625–1651, 1985.

[20] A. L. New and R. D. Pingree, "An intercomparison of internal solitary waves in the Bay of Biscay and resulting from Korteweg-de Vries-type theory," *Progress in Oceanography*, vol. 45, no. 1, pp. 1–38, 2000.

[21] C. R. Jackson, J. C. B. da Silva, and G. Jeans, "The generation of nonlinear internal waves," *Oceanography*, vol. 25, no. 2, pp. 108–123, 2012.

[22] T. Gerkema, "A unified model for the generation and fission of internal tides in a rotating ocean," *Journal of Marine Research*, vol. 54, no. 3, pp. 421–450, 1996.

[23] A. L. New and R. D. Pingree, "Large-amplitude internal soliton packets in the central Bay of Biscay," *Deep Sea Research Part A*, vol. 37, no. 3, pp. 513–524, 1990.

[24] A. L. New and R. D. Pingree, "Local generation of internal soliton packets in the central bay of Biscay," *Deep Sea Research Part A*, vol. 39, no. 9, pp. 1521–1534, 1992.

[25] T. Gerkema, "Internal and interfacial tides: beam scattering and local generation of solitary waves," *Journal of Marine Research*, vol. 59, no. 2, pp. 227–255, 2001.

[26] A. F. Pereira and B. M. Castro, "Internal tides in the southwestern Atlantic off Brazil: observations and numerical modeling," *Journal of Physical Oceanography*, vol. 37, no. 6, pp. 1512–1526, 2007.

[27] A. F. Pereira, B. M. Castro, L. Calado, and I. C. A. da Silveira, "Numerical simulation of M_2 internal tides in the South Brazil Bight and their interaction with the Brazil Current," *Journal of Geophysical Research C*, vol. 112, no. 4, Article ID C04009, 2007.

[28] C. R. Jackson, *An Atlas of Internal Solitary-Like Waves and Their Properties*, Alexandria, Va, USA, 2nd edition, 2004.

[29] B. M. Castro Filho and L. B. Miranda, "Physical oceanography of the Western Atlantic Continental Shelf located between 4°N and 34°S coastal segment," in *The Sea*, K. H. Robinson and K. H. Brink, Eds., vol. 11, pp. 209–251, Wiley, Berlin, Germany, 1998.

[30] B. M. Castro, J. A. Lorenzzetti, I. C. A. Silveira, and L. B. Miranda, "Thermohaline structure and circulation in the region between Cape Sao Tomé and Chui," in *The Oceanographic Environment of the contInental Shelf and Slope in the Southeast-South Region off Brazil*, C. L. Rossi-Wongtschowski and L. S.-P. Madureira, Eds., pp. 11–120, EDUSP, São Paulo, Brazil, 2006.

[31] S. R. Signorini, "On the circulation and the volume transport of the Brazil Current between the Cape of São Tomé and Guanabara Bay," *Deep-Sea Research*, vol. 25, no. 5, pp. 481–490, 1978.

[32] E. J. D. Campos, Y. Ikeda, B. M. Castro, S. A. Gaeta, J. A. Lorenzzetti, and M. R. Stevenson, "Experiment studies circulation in the Western south atlantic," *Eos*, vol. 77, no. 27, pp. 253–259, 1996.

[33] A. R. Piola, O. O. Möller Jr., R. A. Guerrero, and E. J. D. Campos, "Variability of the subtropical shelf front off eastern South America: winter 2003 and summer 2004," *Continental Shelf Research*, vol. 28, no. 13, pp. 1639–1648, 2008.

[34] A. R. de Mesquita and J. Harari, "On the harmonic constants of tides and tidal currents of the South-eastern brazilian shelf," *Continental Shelf Research*, vol. 23, no. 11–13, pp. 1227–1237, 2003.

[35] EUMETSAT, 2012, http://www.eumetsat.int/Home/Main/DataAccess/EUMETSATDataCentre/index.htm?l=en.

[36] SCOW, 2012, http://cioss.coas.oregonstate.edu/scow/.

[37] ETOPO, 2012, http://dss.ucar.edu/datasets/ds759.3/.

[38] G. D. Egbert and S. Y. Erofeeva, "Efficient inverse modeling of barotropic ocean tides," *Journal of Atmospheric and Oceanic Technology*, vol. 19, no. 2, pp. 183–204, 2002.

[39] National Oceanographic Data Centre, 2012, http://www.nodc.noaa.gov/OC5/WOA09/pr_woa09.html.

[40] P. G. Baines, "On internal tide generation models," *Deep Sea Research Part A*, vol. 29, no. 3, pp. 307–338, 1982.

[41] S. T. Dokken, R. Olsen, T. Wahl, and M. V. Tantillo, "Identification and characterization of internal waves in SAR images along the coast of Norway," *Geophysical Research Letters*, vol. 28, no. 14, pp. 2803–2806, 2001.

[42] M. A. Donelan and W. J. Pierson Jr., "Radar scattering and equilibrium ranges in wind-generated waves with application to scatterometry," *Journal of Geophysical Research*, vol. 92, no. 5, pp. 4971–5029, 1987.

[43] P. Brandt, R. Romeiser, and A. Rubino, "On the determination of characteristics of the interior ocean dynamics from radar signatures of internal solitary waves," *Journal of Geophysical Research C*, vol. 104, no. 12, pp. 30039–30045, 1999.

[44] Y. Ouyang, J. Chong, Y. Wu, and M. Zhu, "Simulation studies of internal waves in SAR images under different SAR and wind field conditions," *IEEE Transactions on Geoscience and Remote Sensing*, vol. 49, no. 5, pp. 1734–1743, 2011.

[45] C. G. Justus, W. R. Hargraves, A. Mikhail, and D. Graber, "Methods for estimating wind speed frequency distributions," *Journal of Applied Meteorology*, vol. 17, no. 3, pp. 350–353, 1978.

[46] W. Huang, J. Johannessen, W. Alpers, J. Yang, and X. Gan, "Spatial and temporal variations of internal wave sea surface signatures in the northern south China sea studied by spaceborne SAR imagery," in *Proceedings of the 2nd SeaSAR Symposium*, Frascati, Italy, January 2008.

[47] J. L. Stech and J. A. Lorenzzetti, "The response of the south Brazil bight to the passage of wintertime cold fronts," *Journal of Geophysical Research*, vol. 97, no. 6, pp. 9507–9520, 1992.

[48] S. M. Kelly and J. D. Nash, "Internal-tide generation and destruction by shoaling internal tides," *Geophysical Research Letters*, vol. 37, no. 23, Article ID L23611, 2010.

[49] D. R. G. Jeans and T. J. Sherwin, "The evolution and energetics of large amplitude nonlinear internal waves on the Portuguese shelf," *Journal of Marine Research*, vol. 59, no. 3, pp. 327–353, 2001.

[50] T. J. Sherwin, V. I. Vlasenko, N. Stashchuk, D. R. G. Jeans, and B. Jones, "Along-slope generation as an explanation for some unusually large internal tides," *Deep-Sea Research Part I*, vol. 49, no. 10, pp. 1787–1799, 2002.

[51] O. O. Möller Jr., A. R. Piola, A. C. Freitas, and E. J. D. Campos, "The effects of river discharge and seasonal winds on the shelf off southeastern South America," *Continental Shelf Research*, vol. 28, no. 13, pp. 1607–1624, 2008.

[52] S. V. Babu and A. D. Rao, "Mixing in the surface layers in association with internal waves during winter in the northwestern Bay of Bengal," *Natural Hazards*, vol. 57, no. 3, pp. 551–562, 2011.

[53] M. A. Merrifield and P. E. Holloway, "Model estimates of M_2 internal tide energetics at the Hawaiian Ridge," *Journal of Geophysical Research C*, vol. 107, no. 8, pp. 5–1, 2002.

[54] A. Azevedo, S. Correia, J. C. B. da Silva, and A. L. New, "Hot-spots of internal wave activity off iberia revealed by multisensor remote sensing satellite observations—spotiwave," in *Proceedings of the 2nd Workshop on Coastal and Marine Applications of SAR*, pp. 125–132, Svalbard, Norway, September 2003.

[55] A. Azevedo, J. C. B. da Silva, and A. L. New, "On the generation and propagation of internal solitary waves in the southern Bay of Biscay," *Deep-Sea Research Part I*, vol. 53, no. 6, pp. 927–941, 2006.

[56] J. C. B. da Silva, A. L. New, and J. M. Magalhaes, "Internal solitary waves in the Mozambique Channel: observations and interpretation," *Journal of Geophysical Research-Oceans*, vol. 114, no. C05001, 12 pages, 2009.

[57] J. A. Lorenzzetti, J. L. Stech, W. L. Mello Filho, and A. T. Assireu, "Satellite observation of Brazil Current inshore thermal front in the SW South Atlantic: space/time variability and sea surface temperatures," *Continental Shelf Research*, vol. 29, no. 17, pp. 2061–2068, 2009.

[58] T. Gerkema and J. T. F. Zimmerman, "Generation of nonlinear internal tides and solitary waves," *Journal of Physical Oceanography*, vol. 25, pp. 1081–1094, 1995.

[59] J. Pedlosky, *Waves in the Ocean and Atmosphere. Introduction to Wave Dynamics*, Springer, Berlin, Germany, 2003.

[60] L. L. Fu and B. Holt, "Internal waves in the Gulf of California: observations from a spaceborne radar," *Journal of Geophysical Research*, vol. 89, no. 2, pp. 2053–2060, 1984.

[61] J. Small, Z. Hallock, G. Pavey, and J. Scott, "Observations of large amplitude internal waves at the Malin Shelf edge during SESAME 1995," *Continental Shelf Research*, vol. 19, no. 11, pp. 1389–1436, 1999.

[62] M. Teixeira, A. Warn-Varnas, J. Apel, and J. Hawkins, "Analytical and observational studies of internal solitary waves in the Yellow Sea," *Journal of Coastal Research*, vol. 22, no. 6, pp. 1403–1416, 2006.

[63] J. R. Apel, "Oceanic internal waves and solitons," in *Synthetic Aperture Radar Marine User's Manual*, C. R. Jackson and J. R. Apel, Eds., pp. 189–207, National Oceanic and Atmospheric Administration, Silver Spring, Md, USA, 2004.

[64] A. K. Liu, Y. Steve Chang, M. K. Hsu, and N. K. Liang, "Evolution of nonlinear internal waves in the East and South China Seas," *Journal of Geophysical Research C*, vol. 103, no. 3334, pp. 7995–8008, 1998.

[65] J. C. B. da Silva, A. L. New, and J. M. Magalhaes, "On the structure and propagation of internal solitary waves generated at the Mascarene Plateau in the Indian Ocean," *Deep-Sea Research Part I*, vol. 58, no. 3, pp. 229–240, 2011.

[66] A. R. Osborne and T. L. Burch, "Internal solitons in the Andaman Sea," *Science*, vol. 208, no. 4443, pp. 451–460, 1980.